Pancreatic cancer cells exchange ribosomes through tunnelling nanotubes

Authors

Stanislava Martínková, [1] Denisa Jansová, [2] Jana Vorel, [1] Lucie Josefa Lamačová, [1] Petr Daniel, [1] Michael Hudec, [4] Mário Boďo, [3] Jan Hajer, [5] Andrej Susor, [2] Jan Trnka [1,] *

[1] Department of Biochemistry, Cell and Molecular Biology, Third Faculty of Medicine, Charles University, Prague, Czech Republic

[2] Institute of Animal Physiology and Genetics, The Czech Academy of Sciences, Libechov, Czech Republic

[3] Department of Internal Medicine, Third Faculty of Medicine, Charles University, University Hospital Královské Vinohrady, Prague, Czech Republic

[4] Department of Medical Genetics, Third Faculty of Medicine, Charles University, Prague, Czech Republic

[5] Department of Gastroenterology, Faculty Hospital Bulovka, Prague, Czech Republic

*__Correspondence__: jan.trnka@lf3.cuni.cz (J.T.)

Main points

- pancreatic tumor cells from patient biopsies form tunnelling nanotubes in 2D culture
- formation of tunnelling nanotubes is promoted by gemcitabine
- polyadenylated mRNAs, ribosomal components and assembled ribosomes are present in tunnelling nanotubes
- ribosomes or their components are transferred via nanotubes to acceptor cells

ABSTRACT

Background: Pancreatic ductal adenocarcinoma (PDAC) is considered as one of the deadliest types of cancer. Tunnelling nanotubes (TNTs) are thin, membranous, intercellular communication

structuresobserved in normal and cancer cells, where they mediate the exchange of intracellular material and promote cell fitness, cancer spread and treatment resistance.

Results: PDAC cells increase the formation of TNTs upon exposure to gemcitabine. In the PANC-1 cell line and in tumour explants from patients, we observe polyadenylated mRNA, 5.8S rRNA, ribosomal proteins and assembled 80S ribosomes within the TNTs. Using HaloTag-labelled small ribosomal subunit component RPS9 we demonstrate the transport of ribosomes via TNTs into acceptor cells.

Conclusions: PDAC cells can exchange components of the translational machinery, including mRNA, which may contribute to the resistance to therapy, highlighting the potential of targeting TNT dynamics as a therapeutic approach for PDAC.

KEYWORDS

pancreatic cancer • PDAC • gemcitabine • tunnelling nanotubes • 5.8S rRNA • poly(A) mRNA • ribosomal proteins • ribosomes • translation • chemoresistance

INTRODUCTION

Pancreatic ductal adenocarcinoma (PDAC) is one of the deadliest cancers with a poor prognosis with a five year overall survival rate of approximately 10%.[1] One of the reasons for the aggressive nature of PDAC is its ability to develop chemoresistance, which ultimately leads to treatment failure and disease progression. Detecting this aggressive cancer in its early stages is crucial for successful treatment outcomes. Gemcitabine monotherapy serves as the established standard of care for patients with worse performance status diagnosed with locally advanced and metastatic pancreatic adenocarcinoma.[2] For patients with good performance status, the FOLFIRINOX (oxaliplatin, irinotecan, leucovorin, fluorouracil) regimen is indicated as the method of first choice, as it has shown a significant prolongation of median overall survival.[3]

Due to the rapid proliferation, survival mechanisms, epithelial to mesenchymal transition (EMT), invasiveness, and metastasis, cancer cells are presented with unique metabolic requirements. Pancreatic ductal adenocarcinoma cells, growing in hypoxic conditions and encased within dense stroma, adapt through metabolic reprogramming. This adaptation involves a shift to alternative metabolic pathways to fulfil their energy requirements. Predominantly, these cells upregulate aerobic glycolysis, commonly referred to as the Warburg effect, enhance the hexosamine biosynthetic pathway, activate lipid metabolism, and adapt to the deprivation of essential amino acids.[4] The complex adaptations of cancer cells require a high rate of proteosynthesis[5] and pose strict demands on the capacity of the translation machinery.

The upregulation of ribosome biogenesis is an important characteristic of rapidly dividing cells,[6] EMT, metastasis[7] and also of the stem cell phenotype, where the maintenance of long-term replicative plasticity requires a high rate of ribosome synthesis.[8] Dependence on a high rate of ribosome biogenesis has been

documented also in cancer stem cells and related to poor disease prognosis.[9] The inhibition of rRNA production has been shown to inhibit tumour growth.[10] An inhibitor of RNA polymerase I exhibited antiproliferative activity in cancer cells and tumour xenografts,[11–13] further supporting the importance of ribosomal biogenesis for cancer cell population.

Tunnelling nanotubes (TNTs) are intercellular direct cytoplasmic communication channels that allow cells to transmit signals and cellular components over long distances.[14] Tunnelling nanotubes were first observed in rat pheochromocytoma PC12 cells, as well as in human embryonic kidney cells and normal rat kidney cells. These structures typically had a diameter ranging from 50 to 200 nm and could extend several cell diameters in length. Importantly, they did not lie on the substrate.[15] Typically reported intercellular distances are between ten to several hundred µm.[16,17] TNTs can transport mitochondria,[18] ions,[19] organelle-derived vesicles (endosomes, lysosomes), proteins, non-coding RNA.[18,20–22] Recent studies have documented the role of TNTs in the transmission of SARS-CoV-2.[23] In cancer research, TNTs have been observed transporting mitochondria in glioblastoma patient-derived organoids[24] and in mesenchymal stem cells transferring mitochondria to glioblastoma stem cells and enhancing resistance to temozolomide;[25] in breast cancer cells transferring mitochondria from immune cells.[26] In prostate cancer, TNTs contribute to the adaptation and treatment resistance through mechanisms involving PI3K/AKT signalling, actin remodelling, and the transport of stress-induced proteins;[27] in bladder cancer TNTs connect heterogeneous cells and facilitate the mitochondrial transfer, leading to increased invasiveness both *in vivo* and *in vitro.*[28] The formation of TNTs can also be induced in a dose-dependent manner by doxorubicin *in vitro* with the resulting drug redistribution via TNTs presenting a new addition on cellular mechanisms of drug efflux and the development of drug resistance in cancers.[29] TNT formation can also be triggered by low serum, hyperglycemic, acidic growth medium[30] and hypoxia.[31] TNTs are also known to play a role in tumour progression, invasiveness and metastasis.[28,32,33]

In this study, we investigated how pancreatic ductal adenocarcinoma cells adapt to increasing doses of the chemotherapeutic agent gemcitabine by enhancing the formation of tunnelling nanotubes, and show the transfer of ribosomal components and fully assembled ribosomes in TNTs between PDAC cells in culture.

RESULTS

PDAC biopsy samples develop tunnelling nanotubes in 2D cultures

TNTs have previously been detected in cultures of pancreatic cancer cell lines and tumour tissue sample.[29] We used 2D cultures of patient explants from endoscopic biopsies to see whether cultured primary cancer cells can also form these connections. We assessed the formation of tunnelling nanotubes in three tissue samples obtained from patients diagnosed with pancreatic ductal adenocarcinoma following endoscopic ultrasound-guided fine needle aspiration biopsy. The patients had not undergone any chemotherapy before the biopsy and their characteristics are summarised in Supplementary Table S1. TNTs were observed in all three cultured tissue samples (Figure 1A, Supplementary Figure S1A). Cells started growing out from the biopsy fragments

between 2 to 5 days after plating in a growth medium. All three patients received palliative care. Given that gemcitabine is the most frequently used first-line treatment for palliative chemotherapy in unresectable PDAC, we investigated whether gemcitabine could affect the formation of TNTs in culture.

Gemcitabine induces TNTs formation in PANC-1 in dose-dependent manner

To determine the optimal dosing regimen, we first estimated the IC50 for gemcitabine in PANC-1 cells to be 1.6 µM (Supplementary Figure S1B). The dense stromal composition and poor vascularization characteristic of PDAC hinder effective drug penetration into the tumour *in vivo*, therefore we used sub-IC50 concentrations for further experiments. We exposed PANC-1 cells to three different sub-IC50 doses of gemcitabine: 0.25 µM, 0.5 µM, and 1 µM for 48 hours and observed a dose-dependent stimulation of the formation of tunnelling nanotubes (Figure 1B, 1C), considering only tunnelling nanotubes measuring 20 µm or more in length. The observed tunnelling nanotubes form above the substrate (Figure 1D), as expected from these structures. This observation suggests that sublethal doses of gemcitabine induce the formation of TNTs and potentially influence the survival and growth ability of pancreatic cancer cells.

Messenger RNA, ribosomal components and assembled ribosomes are transported in tunnelling nanotubes

Since rapidly dividing cancer cells are highly dependent on proteosynthesis we hypothesised that RNAs and components of the translation machinery may also be transported through TNTs between PDAC cells. Following a treatment with 0.5 µM gemcitabine for 48 hours to induce the formation of TNTs we detected 5.8S ribosomal RNA (rRNA) within these structures (Figure 2A and Supplementary Figure S2A, S4A). A treatment with RNAse eliminated the RNA signal in the samples (negative control, Supplementary Figure S4B). This rRNA, which is evolutionarily conserved and a critical component of the large subunit of eukaryotic ribosomes, plays an essential role in protein synthesis. Furthermore, we identified 5.8S rRNA within the TNTs between pancreatic ductal adenocarcinoma cells and between stromal cells from a patient's biopsy (Figure 2G, J and Supplementary Figure S2G, J).

We then set out to identify other components of ribosomes in TNTs and found the presence of ribosomal protein S6 and S9 (key components of the 40S subunit) and, ribosomal protein L24 (key component of the 60S subunit) in gemcitabine-activated TNTs in PANC-1 cells (Figure 2B, C, F and Supplementary Figure S2B, C, F) suggesting the possibility that fully assembled ribosomes may be transported between cancer cells via TNTs.

To visualise polyadenylated RNA (mRNA) in tunnelling nanotubes we performed *in situ* hybridization with RNA oligo-d(T) probes (Figure 2D and Supplementary Figure S2D, S5A, RNAse-treated negative control Supplementary Figure S5B). The presence of polyadenylated RNAs complements the detection of ribosomal components and suggests the possibility of transfer of functional ribosomes and mRNA between cells via TNTs.

Complete ribosomes are transferred in TNTs

To investigate whether the presence of 5.8S ribosomal RNA (rRNA), both ribosomal subunits and polyadenylated mRNA within tunnelling nanotubes supports the hypothesis that functional ribosomes can be transferred between cells, we used the proximity ligation assay (PLA) to detect fully assembled, translationally competent ribosomes.[34,35] We used primary antibodies targeting RPL24 and RPS6, spatially close ribosomal proteins from the 60S, respectivelly the 40S ribosomal subunit,[36] to generate a multiplexed fluorescent signal through secondary antibodies with hybridization probes that produced single spots indicative of functional 80S ribosomes (Figure 2E and Supplementary figure S2E, S7A). The assembled ribosomes identified by the RPS6-RPL24 interaction were distributed in the cytoplasm of PANC-1 cells and in intercellular TNTs. The interaction between RPS6 and RPL24 indicates the formation of fully assembled 80S ribosomes and ongoing protein synthesis.[34,35,36] Elimination of assembled ribosomes by a treatment with puromycin,[37] significantly reduced the RPS6-RPL24 PLA signal (Fig 2E and Supplementary figure S7B), confirming the fact that we only obtained signals from assembled ribosomes in the cytoplasm and TNTs (Figure 2E and Supplementary figure S2E, S7A). Our results clearly show that tunnelling nanotubes contain fully assembled ribosomes *en route* between cancer cells.

TNTs are present between primary PDAC cancer cells, fibroblasts from biopsy samples and contain assembled ribosomes

To establish that ribosome transport via tunnelling nanotubes is not exclusive to the PANC-1 cell line but also occurs in primary human pancreatic tumour cells, we cultured primary human PDAC cells in a 2D culture from thin needle biopsy samples. To ascertain the presence of epithelial tumor cells *in vitro*, we used a primary antibody against cytokeratin 19, while the detection of stromal cells was confirmed by a primary antibody against vimentin (Figure 2I, L and Supplementary Figure S2I, L). One patient sample (sample 26) was positive for epithelial cells, while the other (sample 24) contained vimentin-positive stromal fibroblasts without any cytokeratin signal. Both patient samples expanded in culture and formed TNTs, which, interestingly, contained significant signals of the two intermediate filament proteins, cytokeratin-19 or vimentin, respectively. Using the RPS6-RPL24 proximity ligation assay we detected assembled ribosomes in these TNTs (Figure 2H, K and Supplementary Figure S2H, K). These data show that functional assembled ribosomes are present in TNTs of primary PDAC cells, as well as in those formed between primary stromal cells.

Ribosomal components and assembled ribosomes are transported from donor cells to acceptor cells via TNTs

To demonstrate that ribosomal components are transported from donor to acceptor cells via gemcitabine-activated TNTs, inspired by Gallo *et al.*,[38] we generated PANC-1 cells transfected with a mammalian expression vector encoding the human small ribosomal subunit RPS9, C-terminally tagged with HaloTag (donor cells). These transfected donor cells expressed tagged RPS9 in the nucleolus, nucleus, and cytoplasm (Supplementary Figure S3E), and a time-lapse video shows the movement of the labelled ribosomal component (Video 1).

Acceptor cells were stably labelled either by staining with the covalent CellTrace Violet stain (CellTrace Violet+) or by a transfection with GFP with NLS localized in the nucleus. After washing and trypsinization, equal numbers of donor and acceptor cells were seeded and cultured in 24-well plates. Next, co-cultured donor and acceptor cells were treated by with gemcitabine for two days to induce the formation of TNTs. Subsequently, the cells were stained with HaloTag-TMR ligand (HaloTag TMR+), allowing for the observation of double-stained cells, in some cases with a TNT connecting a HaloTag positive donor cell with an acceptor cell. These observations strongly suggest that HaloTag-RPS9 was exchanged between the two cell populations through the TNTs (Figure 3A, B and Supplementary Figure S3A, B).

To confirm our hypothesis that the intercellularly transferred HaloTag-RPS9 subunits are incorporated into complete ribosomes we first performed the RPS9-RPL24 proximity ligation assay to ascertain the necessary close proximity of these two subunits (Figure 3C and Supplementary Figure S3C). Next, we performed anti-HaloTag-anti-RPL24 proximity ligation assay to see whether the transgenic RPS9 subunits are also incorporated into 80S ribosomes (Figure 3D and Supplementary Figure S3D). Finally, we mixed HaloTag-RPS9 transfected cells with untransfected CellTrace Violet-stained cells and performed the anti-HaloTag-anti-RPL24 proximity ligation assay. The positive PLA signal in CellTrace Violet-stained acceptor cells (Figure 3E and Supplementary Figure S8) is a clear evidence for complete ribosomes in the Violet cells containing the HaloTag-RPS9 subunit transferred from the donor cells, which strongly supports our hypothesis. A negative control with cells without the HaloTag-RPS9 transgene is shown in Supplementary Figure S9.

To support further the evidence for the transport of ribosomal components from donor to acceptor cells we used flow cytometry to quantify double-positive (HaloTag TMR+ and CellTrace Violet+) cells formed in a mixed population of HaloTag-RPS9 transgenic donor cells and untransfected CellTrace Violet labelled acceptor cells (Figure 3F). The exposure to gemcitabine increases somewhat the number of double-stained cells, which is consistent with our observations above regarding the stimulation of TNT formation by this drug and with the hypothesis that TNTs are the conduit for transferring ribosomal components between cells.

DISCUSSION

Our results show that ribosomal components 5.8S rRNA, RPS9, RPS6, RPL24, and fully assembled ribosomes together with mRNA are present in TNTs between pancreatic cancer cells, and that they are transported between cells. These findings expand the current knowledge about the nature of intracellular material transported in TNTs and show a possible new direction in cancer biology research.

As stated in the Introduction, ribosomal biogenesis has been shown as one of key determinants of cancer cell survival, proliferation, adaptation and spread leading to the development of specific inhibitors of rRNA synthesis as possible anticancer agents.[10] Currently used chemotherapeutic agents have also been shown to inhibit rRNA synthesis and ribosome biogenesis, which may contribute to their anticancer effects.[39] Since the intercellular transfer of mitochondria has been proposed as an adaptive mechanism capable of restoring defective mitochondrial function in acceptor cells,[40–43] it is perhaps not too far-fetched to see the potential

adaptive impact of ribosome transport in cancer cells, which are in many instances dependent on an upregulated rate of ribosome biogenesis and proteosynthesis. The formation of TNTs and their enabling of the transfer of ribosomes and gene transcripts may be part of the response to chemotherapy-induced cellular stress and contribute to the survival of acceptor cells.

Our results show that sub-IC50 concentrations of gemcitabine induce the formation of TNTs between cancer cells. Since TNTs provide the means of redistributing intracellular components from one cell to another, in the case of mitochondria with a proven adaptive impact,[18,25,26] it is possible to see the induction of TNT formation by gemcitabine as a potential contributor to chemoresistance. The fact, reported in the present study, that ribosomes and ribosomal components are also transferred between cells may further contribute to this pro-survival and pro-proliferative potential of TNT formation.

The phosphorylation of RPS6 via an aberrant activation of the mTOR pathway is a significant factor in the initiation and progression of pancreatic cancer[44] and is related to metastasis and poor prognosis in other types of cancer,[45] which presents a possible therapeutic target.[46] Studies have also shown that the inhibition of mTORC1 decreases the proliferative ability of PDAC cells *in vitro* and *in vivo,*[47] and the chemosensitivity to gemcitabine potentiated by inhibiting proteosynthesis.[48] The apparent dependence of PDAC cells on RPS6 phosphorylation and increased rate of proteosynthesis may indicate a further adaptive use for the transfer of ribosomes between cells with different S6 kinase activities and ribosomal pools due to different nutrient status, growth factor signalling cascade activation, cellular stress levels or other factors.

Immunocytochemistry used in this study detects individual ribosomal components with the exception of the proximity ligation assay, which relies on the proximity of two proteins located in the small and large ribosomal subunit and produces signal only if the two subunits are close together. While our data show that complete 80S ribosomes are present in TNTs and exogenous HaloTag-RPS9 subunits are seen in complete 80S ribosomes in untransfected acceptor cells, we cannot exclude the possibility that in addition to assembled ribosomes TNTs transport individual ribosomal components that are later formed into ribosomes in the reciepent cell. Rustom *et al.*,[15] showed that TNTs impede the transfer of small molecules including small proteins such as monomeric GFP (~27 kDa). Since several ribosomal components including RPS9 (22.5 kDa) are similar in size or smaller than GFP we can conclude that their transport is unlikely unless they are incorporated into larger complexes or even complete ribosomes.

While the TNT-mediated intercellular transfer of cytosolic components other than ribosomes has been previously shown[18,20–22] the precise mechanisms driving these movements are still poorly characterised. The importance of the actin cytoskeleton for TNT formation and TNT-mediated transport is clear from numerous studies[15,49] with recent reports implicating both actin and tubulin-linked motors in the transport.[50] Whether ribosomes or their components are equipped with suitable adaptors for such cytoskeleton-based transport remains to be shown. While we detected ribosomes and ribosomal components in TNTs we cannot exclude the possibility that other means of intercellular transport may occur simultaneously, e.g. via extracellular vesicles.[51,52]

The trafficking of ribosomes and RNA and the associated regulation of translation between cancer cells may be another factor contributing to their resilience and adaptability, highlighting the pro-survival strategies that negatively influence cancer treatment. The mechanisms of ribosomal and mRNA transport via TNTs, its regulation and detailed effects of the transferred ribosomes and RNAs in the acceptor cells need to be further investigated in order to expand the possibilities for the treatment of patients with cancer. Since we have observed the formation of TNTs in both stromal cells and cancer cells, a detailed study of the heterotypic exchange of ribosomes within the tumour could provide further insights into the complex relationships between malignant and supporting cells.

METHODS

Experimental model and subject details

Isolation of patients' PDAC samples from EUS-guided FNAB

Patient samples were collected using fine-needle aspiration biopsy under endoscopic ultrasound (EUS-FNAB) control, which is the standard method for diagnosing pancreatic cancer. A mandrel aspiration needle was employed for the biopsy and removed after insertion into the lesion. Subsequently, several passes of the needle through the fixed lesion were performed under a vacuum, induced by a syringe with a fixable plunger position. The aspirate obtained by needle aspiration was transferred into a collection container with a transfer medium and into another container for cytological examination by the pathologist. Patient preparation for the procedure was similar to other therapeutic upper gastrointestinal endoscopies or biopsies of other abdominal organs. Patients arrived fasting, were informed about the purpose of the examination and its procedures, and provided their consent by signing an informed consent form. Standard analgosedation was used during the examination, and premedication with antibiotics was administered during the biopsy of cystic lesions. Patients were examined lying on their left side, with the possibility of additional position adjustments. Heart rate, blood pressure, and blood oxygen saturation were monitored throughout the procedure. The conclusion of the results, determined by the diagnostic pathologist, was based on the tissue samples examined in our study.

Cultivation of primary PDAC cells from biopsy tissues in 2D culture

Following EUS-FNAB, fresh patient-derived samples were immediately transferred into transfer medium (TM) composed of DMEM/F-12 Ham nutrient mixture, 10% foetal bovine serum (FBS), 1% Penicillin/Streptomycin, and 50 µg/mL Primocin at final concentrations, and transported on ice to the laboratory. Tissues were transferred using a pre-wetted pipette and tweezers onto a sterile glass Petri dish containing drops of wash medium with the same composition as the transfer medium. The tissue underwent five rounds of washing, with each round involving the gradual transfer of the tissue to new drops of wash medium. Subsequently, the tissue samples were minced into smaller fragments measuring 1–2 mm^3 each using a scalpel in a separate drop of wash medium. These tissue fragments were then placed at the centre of a 12-well plate, pre-coated with rat tail collagen, and submerged in pre-warmed growth Biojepan culture medium (BCM). The BCM culture medium consisted of DMEM/Nutrient Mixture F-12 Ham, 2% foetal bovine serum, 2 mM GlutaMAX, 1%

Penicillin/Streptomycin, 5 µg/mL insulin, 10 ng/mL epidermal growth factor, 0.4 µg/mL hydrocortisone, 10 µM Y-27632, and 50 µg/mL Primocin at final concentrations. The plate was transferred to an incubator set at 37°C and 5% CO_2. The growth BCM medium was refreshed every 2–3 days.

Pancreatic cancer tissue was obtained from patients undergoing tissue biopsies at University Hospital Kralovske Vinohrady in Prague. Written informed consent was obtained from all patients. The study was approved by the Ethics Committee of the University Hospital Kralovske Vinohrady (EK-VP/05/0/2023) and adhered to the Declaration of Helsinki.

PANC-1 cultivation and cell viability assay

PANC-1 cells were seeded at a density of six hundred viable cells per well in a 96-well plate and cultured in 100 µL of DMEM supplemented with 10% foetal bovine serum (FBS) and 1% Penicillin/Streptomycin (complete DMEM medium) at 37°C and 5% CO_2. For the viability assay and determination of IC50 the medium was replaced after 24 hours of cultivation with a medium supplemented with varying concentrations of gemcitabine. Each experiment was set up in technical triplicates with gemcitabine concentration ranging from 1.0×10^{-8} to 1.0×10^{-4} mol/L. After 3 days of treatment, cell viability was assessed using CellTiter-Glo as per the manufacturer's instructions, and relative luminescence units were measured using the TECAN Infinite M200Pro microplate reader. The measured values of luminescence were obtained from three independent experiments, and the data were recorded for analysis. The dose-response model was created using the *drc* package with a four-parameter log-logistic function and the minimum fixed at 0 and the maximum fixed at the untreated control. The dose-response curve is in Supplementary Figure S1B, and data and R script available at https://github.com/trnkaj/ribosomes.

PANC-1 TNTs activation and counting

The human PANC-1 cell line was cultured as described above. For the dose-response curve of TNT numbers vs. gemcitabine concentration we exposed cells to 0.25 µM, 0.5 µM, and 1 µM of gemcitabine for 2 days. The F-actin in live cells was stained using CellMask Green Actin Tracking Stain to detect TNTs in both the control and gemcitabine-treated groups. TMRM was used for staining mitochondria at a final concentration of 100 nM. Hoechst 33342 cell-permeant nuclear counterstain was applied at a final concentration of 5 µg/mL for cell counting purposes. The cells were then incubated with the staining solutions for 30 minutes at 37°C in a 5% CO_2 incubator.

Four random regions of interest (ROIs) were selected, and scanning was performed using a Plan Fluor 4x objective (0.13 NA) in DAPI, FITC and TRITC field modes. Imaging was conducted with a monochrome pco.panda 4.2 camera mounted on the camera port of a Nikon Eclipse Ts2 fluorescence inverted manual microscope. TNTs in both control and treated cells were counted in four independent images. The number of TNTs at each concentration of gemcitabine was normalised to 1×10^4 cells. For nuclear counting and TNT detection, NIS-AR Elements software was used. Measurements were obtained from three independent experiments, and the data were recorded for analysis.

For analyses of ribosomal components, we exposed PANC-1 cells to 0.5 µM gemcitabine for 48 hours prior to microscopy. Patient-derived cells were not exposed to gemcitabine.

Bayesian linear model of dose-dependence

We use a linear model to estimate the dose-dependence of TNT formation on gemcitabine concentration. The model:

$$y_i \sim Normal(\mu, \sigma)$$

$$\mu_i = \alpha + \beta x_i$$

$$\alpha \sim Normal(0,1)$$

$$\beta \sim Normal(0,1)$$

$$\sigma \sim Exponential(1)$$

used normalised values of the number of TNTs (*y*) and gemcitabine concentration (*x*) and was estimated using the weakly informative priors with STAN via the *rethinking* package by Richard McElreath. The source data and R code are available at https://github.com/trnkaj/ribosomes

Immunocytochemistry of ribosomal components

The PANC-1 cell line was treated for 2 days with 0.5 µM gemcitabine for TNT activation. PDAC primary cells isolated from EUS-FNAB patient samples were grown on a cover glass for immunofluorescence purposes. The samples were fixed in 4% paraformaldehyde (PFA) in phosphate-buffered saline (DPBS) pH 7.4 for 15 minutes at room temperature (RT). The samples were then washed three times in 1% BSA/DPBS, each lasting 5 minutes, and permeabilized for 20 minutes with 1% BSA/DPBS containing 0.1% Triton X-100 at RT. Afterward, cells were washed three times for 5 minutes each in 1% BSA/DPBS and blocked using a solution of 1% BSA/DPBS to prevent non-specific antibody binding. After 1 hour of blocking, primary antibodies were added and diluted in 1% BSA/DPBS. The cells were then incubated with primary antibodies overnight (O/N) in a humidified chamber at 4°C. The following primary antibodies were used: anti-rRNA antibody (Immunogen: whole 5.8S ribosomal RNA), anti-RPS6 antibody, anti-RPS9 antibody, anti-RPL24 antibody, anti-vimentin antibody, and anti-cytokeratin 19 antibody. Subsequently, the samples underwent three 10-minute washes, and were then incubated with the relevant Alexa Fluor 488/546/647 conjugated secondary antibody for 2 hours at RT in the dark. Following the incubation, the samples were rinsed three times with 1% BSA/DPBS for 10 minutes each. ActinGreen™ 488 ReadyProbes or ActinRed™ 555 ReadyProbes were used for F-actin staining. Subsequently, the samples underwent another three washes with 1% BSA/DPBS before being mounted in VECTASHIELD® Antifade Mounting Medium with DAPI.

RNA fluorescent in situ hybridization (FISH) – Poly(A) mRNA

Cells with activated TNTs, seeded on cover glass, were fixed for 15 minutes in 4% PFA and permeabilized with 1% Triton X-100 in DPBS. The samples were washed in 900 µL of 1× wash buffer A and incubated O/N at 42°C in a hybridization buffer with 75 nM oligo-d(T) probe and CalFluorRed635. The samples were then washed twice in wash buffer A and twice in 2× SSC. ActinGreen™ 488 ReadyProbes was used for F-actin staining according to the manufacturer's instructions. Finally, the samples were mounted in VectaShield medium with DAPI.

Negative controls for 5.8S rRNA and for Poly(A) mRNA

RNase treatments were employed as negative controls to validate the specificity of the anti-5.8S rRNA antibody and the FISH Poly(A) assay. These controls were used to confirm the binding affinity of the rRNA monoclonal antibody and the oligo-d(T) probe. PANC-1 cells with activated TNTs were fixed in 4% PFA for 15 minutes at room temperature (RT), washed twice with DPBS, and incubated with an RNase mix (RNase A, RNase H, and RNase III in 500 µL DPBS) for 2 hours at 37°C. After incubation, the cells were thoroughly washed with DPBS to remove residual RNases. The procedure was then continued with immunocytochemistry or RNA FISH. Specificity of the Alexa Fluor™ Plus 647 secondary antibody was assessed using negative controls to differentiate specific binding from non-specific signals. Subtraction of non-specific signals from experimental images enabled accurate quantification of fluorescence corresponding to the binding of primary antibodies to their targets.

Cloning of HaloTag-RPS9

For the cloning strategy, total RNA was isolated from MCF-7 breast cancer cells (RRID: CVCL_0031) using the RNeasy Kit according to the manufacturer's instructions. Two micrograms of total RNA were reverse transcribed by oligo$(dT)_{18}$ in a 20 µL reaction using the Maxima H Minus First Strand cDNA Synthesis Kit following a modified protocol: 50°C for 30 minutes followed by 55°C for 30 minutes. Then, cDNA equivalent to 20 ng of mRNA served as a nested PCR template in a total volume of 50 µL. The first PCR was done with the CLO_hsRPS9_FOR and CLO_hsRPS9_REV pair of primers specific to the 5' and 3' untranslated regions of human RPS9. Primers for the second PCR, CLO_hsRPS9Eco_FOR and CLO_hsRPS9Xho_REV were situated to encompass RPS9 open reading frame except the stop codon. Both PCR reactions ran for 35 cycles with Q5 high-fidelity polymerase under similar conditions: initial denaturation at 95°C for 2 minutes, denaturation at 95°C for 20 seconds, annealing 63.8°C for 20 seconds, extension at 72°C for 40 seconds and final extension at 72°C for 3 minutes. The product of the second PCR was cloned via *Eco*RI and *Xho*I sites in frame with the C-terminal Halo® Tag to generate pHTC-hsRPS9-HaloTag® CMV-neo vector (Supplementary figure S10). The insert was sequenced using CMV universal sequencing primer CMV_FOR.

Transfection of HaloTag-RPS9

The PANC-1 cell line was cultured in complete DMEM medium at 37°C with 5% CO_2. Upon reaching 70% confluence on a 24-well plate, the cells were transfected with the pHTC-hsRPS9-HaloTag® CMV-neo vector using Lipofectamine™ 3000 Transfection Reagent (donor cells) according to the manufacturer's instructions. Two days after transfection, the medium was replaced with fresh complete DMEM.

Transport of HaloTag-RPS9 do acceptor cells

Two stained variants of PANC-1 acceptor cells were used: one with the nucleus stained using the CellLight™ Nucleus-GFP BacMam 2.0, and the other with the entire cell stained using the covalent CellTrace™ Violet Cell Proliferation Kit, both following the manufacturer's instructions. Expressed RPS9 (in donor cells) was visualised by staining live cells with the HaloTag-TMR ligand for 30 minutes in an incubator at 5% CO□ before the co-culture experiment. The wells containing donor and acceptor cells were washed with pre-warmed DPBS at 37°C prior to trypsinisation and centrifugation. Subsequently, the centrifuged cells were washed twice

separately with pre-warmed DPBS and resuspended in complete DMEM medium. Donor and acceptor cells were then mixed in equal proportions and seeded onto cover-glasses in a 24-well plate. One day post-seeding, the cells were treated with 0.5 µM gemcitabine to activate TNTs for two days. After the three-day co-culture, expressed RPS9 was visualised by re-staining live cells with the HaloTag-TMR ligand, fixed for 15 minutes in 4% PFA in DPBS, and actin was stained with CellMask™ Green Actin Tracking Stain in DPBS for 30 minutes at room temperature in the dark. Cells were then washed three times with DPBS before being mounted in VECTASHIELD without DAPI and imaged using a fluorescence microscope and a confocal microscope. For live cell microscopy, the cells were stained with HaloTag® TMR Ligand to detect expressed RPS9 from the vector. Live cell video of transport of HaloTag- RPS9 was recorded using a Leica Stellaris 8 confocal microscope.

Proximity ligation assay (PLA) of 80S ribosome complex, RPS6-RPL24, RPS9-RPL24 and HaloTag-RPS9-RPL24

The PANC-1 cell line with activated TNTs, seeded on cover glass, was fixed for 15 minutes in 4% PFA in DPBS and permeabilized for 20 minutes in 0.1% Triton X-100 in DPBS. The PLA Duolink kit blocking solution was then added to the sample. For the three types of PLA experiments, three different combinations of the primary antibody were used. For the first variant, the cells were incubated with primary antibodies rabbit anti-RPL24 (1:100) and mouse anti-RPS6 (1:150) at 4°C O/N. For the second variant, anti-RPL24 (1:100) and mouse anti-RPS9 (1:150) were used. For the third variant, anti-RPL24 (1:100) and Anti-HaloTag® Monoclonal Antibody (1:250) were used. The samples were washed in DPBS and then in Wash Buffer A. They were incubated with 240 µL of reaction mixture (48 µL PLA probe MINUS stock, 48 µL PLA probe PLUS stock and 144 µL DPBS) in a chamber for 1 hour at 37°C. The cells were washed in 1× Wash Buffer A for 6 × 2 minutes, followed by ligation performed in 240 µL of reaction mixture containing 6 µL of ligase, 48 µL of ligation buffer, and 186 µL of molecular H_2O. Samples were incubated in the ligation reaction mixture for 30 minutes at 37°C and then washed 6 × 2 minutes in Wash Buffer A. Next, 240 µL of amplification reaction mixture (3 µL polymerase and 48 µL amplification solution) was added to each sample before incubation at 37°C for 100 minutes. The samples were washed in 500 µL of Wash Buffer B for 3 × 5 minutes and 1 × 2 minutes in 0.01× Wash Buffer B. ActinRed™ 555 ReadyProbes was used for F-actin staining according to the manufacturer's instructions. Finally, the samples were mounted using VECTASHIELD® Mounting Medium with DAPI. For the PLA assays, three combinations were used: one detecting the interaction between RPL24 and RPS6, the second detecting the interaction between RPL24 and RPS9, and the third aimed at detecting the interaction between RPL24 and RPS9 expressed from the pHTC-hsRPS9-HaloTag® CMV-neo vector. As a negative control for the PLA assay we treated PANC-1 cells with activated TNTs with puromycin at a final concentration of 10 µg/mL for 4 hours to cause ribosome disassembly. After treatment, the cells were fixed in 4% PFA for 15 minutes at RT, washed twice with DPBS, and the PLA experiment using primary antibodies anti-RPS6 and anti-RPL24 was performed.

Incorporation of HaloTag-RPS9 into ribosomes of acceptor cells

To demonstrate the incorporation of HaloTag-RPS9 into the ribosomes of acceptor cells, acceptor cells labelled with CellTrace Violet were co-cultured with donor cells transfected with the pHTC-hsRPS9-HaloTag vector, as mentioned in the methods above. One day post-seeding, the cells were treated with 0.5 µM gemcitabine to activate TNTs for two days. After the three-day co-culture, cells were stained with the HaloTag-TMR ligand and fixed in 4% PFA in DPBS before undergoing a proximity ligation assay (PLA) using anti-HaloTag and RPL24 primary antibodies. After the PLA, cells were stained for actin using CellMask™ Deep Red Actin. VECTASHIELD without DAPI was used for mounting, and the cells were subsequently imaged using a confocal microscope. Negative control for experiment was performed. Mixed CellTrace™ Violet-labelled cells and non-stained PANC-1 cells were fixed in 4% PFA for 15 minutes at RT after two days of co-culturing, washed twice with DPBS, and used to validate the specificity of the Anti-HaloTag® Monoclonal Antibody and the HaloTag® TMR Ligand staining. The PLA assay (Anti-HaloTag and anti-RPL24) and TMR-Ligand staining were conducted on cells lacking the HaloTag-RPS9 transgene. Actin was stained using CellMask™ Deep Red Actin. VECTASHIELD without DAPI was used for mounting, and cells were subsequently imaged by confocal microscopy.

Fluorescence and confocal microscopy

For scanning fluorescently labelled samples, a Leica Stellaris 8 confocal microscope (indicated by * in image labels) and a Nikon Eclipse Ts2 fluorescence inverted manual microscope (indicated by # in image labels) were used. An inverted routine fluorescence microscope (Nikon Eclipse Ts2) was equipped with Plan Fluor 4x objective (0.13 NA), Plan Fluor 10x objective (0.30 NA), S Plan Fluor ELWD 20x objective (0.45 NA) and S Plan Fluor ELWD 40x objective (0.60 NA). Next, an inverted confocal microscope (Leica Stellaris 8) with a typeG-immersion liquid 40x objective (1.25 NA) was used for sample visualisation. The inverted microscope, equipped with a controlled chamber system (Temp Controller 2000–2, Pecon and a CO_2 Controller, Pecon), was used for time-lapse recordings. The images were processed using NIS-Elements Advanced Research, Leica Application Suite (LAS X), and ImageJ/FIJI.

Flow cytometry

For the dual cell labelling experiment, PANC-1 cells were cultured to 80–90% confluency and then transfected with the HaloTag-RPS9 plasmid using Lipofectamine transfection reagent. Forty-eight hours post-transfection, cells expressing HaloTag-RPS9 were stained with TMR ligand to verify transfection efficiency. Before mixing donor and acceptor cells, donor cells (HaloTag-RPS9) and acceptor cells (CellTrace Violet) were washed with pre-warmed DPBS, centrifuged, washed twice separately with pre-warmed DPBS and resuspended in complete DMEM medium. Cells were combined and seeded into a 24-well plate at equal numbers. Two conditions were set up for the mixed culture: an untreated control and a group treated with 0.5 µM gemcitabine for 24 hours. Following incubation, cells expressing HaloTag-RPS9 were stained with TMR ligand for 30 minutes at 37°C to ensure accurate signal detection. All cells were then fixed in the dark with 4% PFA for 15 minutes at room temperature, centrifuged, washed twice with DPBS, and resuspended in 500 µl of DPBS for flow cytometry.

Cytometry data were analysed using an R script available at https://github.com/trnkaj/ribosomes. Data. fcs files generated by BD FACSuite™ Software (BD Biosciences, CA, USA) were read using the *flowCore* and *ggcyto* packages by Bioconductor.[53,54] All measured events for each experimental condition were gated using a maximum FSC-W value to remove doublets, which could present themselves as double-stained cells. Minimum fluorescence intensity values for selecting HaloTag TMR and CellTrace Violet positive events were chosen using fluorescence values of fluorescence minus one (FMO) control cells. Specifically, for the HaloTag/CellTrace Violet mixed population experiments the DAPI channel signal of cells containing HaloTag-RPS9 with TMR ligand was used to set the CellTrace Violet positive gate as any value over the maximum DAPI channel value in these control cells, and PE channel fluorescence of cells stained with CellTrace Violet was used to set the HaloTag TMR positive gate as any value over the maximum PE channel value in these control cells. Events in FMO controls with fluorescence intensity over ten standard deviations above the log-mean were ignored in the setting of fluorescence intensity gates. As double-positive cells we considered cells with fluorescence values in both channels higher than the respective fluorescence minus one control. Since the doublet gate (FSC-W) is likely to have a substantial effect on the total number of double-stained cells observed, we performed a sensitivity analysis by varying the value of this gate over the range of available events and observing the changes in the resulting number of double-positive cells (Supplementary Figure S11).

Antibodies	**Source**	**Code**
rRNA Monoclonal Antibody (Y10b)	Thermo Fisher	MA1-16628
RPL24 Polyclonal Antibody	Invitrogen™, Thermo Fisher	PA5-62450
Ribosomal Protein S6 Antibody (C-8)	Santa cruz biotechnology	sc-74459
Anti-HaloTag® Monoclonal Antibody	Promega	G9211
Anti-Vimentin antibody	Abcam	ab92547
Anti-Cytokeratin 19 antibody	Abcam	ab9221
Donkey anti-Rabbit IgG (H+L) Highly Cross-Adsorbed Secondary Antibody, Alexa Fluor™ 488	Invitrogen™, Thermo Fisher	A-21206
Goat anti-Mouse IgG (H+L) Cross-Adsorbed Secondary Antibody, Alexa Fluor™ 546	Invitrogen™, Thermo Fisher	A-11003
Goat anti-Rabbit IgG (H+L) Highly Cross-Adsorbed Secondary Antibody, Alexa Fluor™ 647	Invitrogen™, Thermo Fisher	A-21245
Goat anti-Mouse IgG (H+L) Highly Cross-Adsorbed Secondary Antibody, Alexa Fluor™ Plus 647	Invitrogen™, Thermo Fisher	A32728
Chemicals	**Source**	**Code**
DMEM/Nutrient Mixture F-12 Ham	Sigma-Aldrich	D6434
DMEM, low glucose, pyruvate	Gibco™ Thermo Fisher	31885-023
DPBS, no calcium, no magnesium	Gibco™ Thermo Fisher	14190144
Fetal Bovine Serum, qualified, Brazil	Gibco™ Thermo	10270106

	Fisher	
GlutaMAX™ Supplement	Gibco™ Thermo Fisher	35050061
Penicillin-Streptomycin	Sigma-Aldrich	P4333
Primocin® Antimicrobial agent for primary cells	InvivoGen	Ant-pm-1
Insulin, human recombinant, zinc solution	Gibco™ Thermo Fisher	12585014
Human EGF Recombinant Protein	Gibco™ Thermo Fisher	PHG0311
Hydrocortisone, 98%, Thermo Scientific Chemicals	Thermo Scientific Chemicals	A16292.03
Y-27632 (dihydrochloride)	MedChemExpress	129830-38-2
Trypsin-EDTA (0.5%), no phenol red	Gibco™ Thermo Fisher	15400054
Collagen I, rat tail	Gibco™ Thermo Fisher	A1048301
Acetic acid	Sigma-Aldrich	V800019
Gemcitabine hydrochloride, 98%	Thermo Scientific Chemicals	461060010
Paraformaldehyde	Sigma-Aldrich	158127-100G
Triton™ X-100	Sigma-Aldrich	T8787
Bovine Serum Albumin	Sigma-Aldrich	A7030-100G
Nuclease-Free Water (not DEPC-Treated)	Invitrogen™ Thermo Fisher	AM9937
Stellaris® RNA FISH Hybridization Buffer	Biosearch Technologies	SMF-HB1-10
Stellaris® RNA FISH Wash Buffer A	Biosearch Technologies	SMF-WA1-60
Stellaris® RNA FISH Wash Buffer B	Biosearch Technologies	SMF-WB1-20
SSC Buffer 20× Concentrate	Sigma-Aldrich	S6639
Hoechst 33342	Invitrogen™ Thermo Fisher	H1399
Vectashield Vibrance® Antifade Mounting Medium with DAPI	Vector Laboratories	H-1800
VECTASHIELD® Antifade Mounting Medium	Vector Laboratories	H-1000-10
CellMask™ Green Actin Tracking Stain	Invitrogen™ Thermo Fisher	A57243
CellMask™ Deep Red Actin Tracking Stain	Invitrogen™ Thermo Fisher	A57245
ActinGreen™ 488 ReadyProbes™ Reagent (AlexaFluor™ 488 phalloidin)	Invitrogen™ Thermo Fisher	R37110
ActinRed™ 555 ReadyProbes™ Reagent (Rhodamine phalloidin)	Invitrogen™ Thermo Fisher	R37112
HaloTag® TMR Ligand	Promega	G8251
CellLight™ Nucleus-GFP, BacMam 2.0	Invitrogen™ Thermo Fisher	C10602
CellTrace™ Violet Cell Proliferation Kit, for flow cytometry	Invitrogen™ Thermo Fisher	C34571
Q5® High-Fidelity DNA Polymerase	NEB, Ipswich	M0491S

Ambion™ RNase A, affinity purified, 1 mg/mL	Invitrogen™ Thermo Fisher	AM2270
ShortCut® RNase III, 2,000 units/m	New England Biolabs	M0245S
RNase H (5 U/µL)	Thermo Scientific™ Thermo Fisher	EN0202
Leica Biosystems Glycerine	Leica Biosystems	11513910
Assays and Kits	**Source**	**Code**
CellTiter-Glo Luminescent Cell Viability Assay	Promega	G7571
Duolink® In Situ PLA® Probe Anti-Rabbit MINUS	Sigma-Aldrich	DUO92005
Duolink® In Situ PLA® Probe Anti-Mouse PLUS	Sigma-Aldrich	DUO92001
Duolink® In Situ Detection Reagents Green	Sigma-Aldrich	DUO92014
Duolink® In Situ Wash Buffers, Fluorescence	Sigma-Aldrich	DUO 82049
Lipofectamine™ 3000 Transfection Reagent	Invitrogen™ Thermo Fisher	L3000001
RNeasy Mini Kit (50)	Qiagen	74104
Maxima H Minus First Strand cDNA Synthesis Kit	Thermo Scientific™ Thermo Fisher	K1652
Opti-MEM Reduced Serum Medium	Gibco™ Thermo Fisher	31985-062
Oligonucleotides	**Source**	**Code**
Polydt proba cy5- Sequence: NTTTTTTTTTTTTTTTTTTTT	biotech genery costume probe	1351P3
CLO_hsRPS9_FOR (5'-GGTGGTTTGCTTAGGCGCAGACG-3')	first PCR custome primer, Sigma-Aldrich	VC00021N
CLO_hsRPS9_REV (5'-GAGACAATCCAGCAGCCCAGGAG-3')	first PCR custome primer, Sigma-Aldrich	VC00021N
CLO_hsRPS9Eco_FOR (5'-ATATAAT*GAATTC*ACCATGCCAGTGGCCCGGAGCTG-3')	cloning second PCR custom primer, Sigma-Aldrich	VC00021N
CLO_hsRPS9Xho_REV (5'-AATAGTA*CTCGAG*ATCCTCCTCCTCGTCGTCTCC-3')	cloning second PCR custom primer, Sigma-Aldrich	VC00021N
Biological samples and experimental cell line	**Source**	**Code**
Human patient samples	University Hospital Kralovske Vinohrady, Prague	N/A
PANC-1 Cell Line	Sigma-Aldrich	87092802-1VL
Recombinant DNA	**Source**	**Code**
pHTC HaloTag® CMV-neo-Vector	Promega	G7711
pHTC-hsRPS9-HaloTag® CMV-neo	This paper	N/A
Culture Plastics and Cover glass	**Source**	**Code**
Nunc™ Cell-Culture Treated Multidishes	Thermo Scientific™ Thermo Fisher	150628

Nunc™ Cell-Culture Treated Multidishes	Thermo Scientific™ Thermo Fisher	142475
Nunc™ MicroWell™ 96-Well, Nunclon Delta-Treated	Thermo Scientific™ Thermo Fisher	136101
Round cover glasses, Menzel Gläser 12 mm Ø, # 1.5	Epredia™ Menzel™, Fisher Scientific	MENZCB00120RAC20
Laboratory instruments	**Source**	**Code**
Infinite M200Pro microplate reader	TECAN	equipment
Nikon Eclipse Ts2 fluorescence microscope	Nikon	equipment
Leica confocal microscope Stellaris 8	Leica	equipment
BD FACSVerse™	BD Biosciences	equipment
Software	**Source**	**Code**
NIS-elements	Nikon	AR 5.20.00
R version 4.4.0 (2024-04-24)	The R Project for Statistical Computing	https://www.r-project.org/
Leica Application Suite X (LAS X)	Leica	LAS X 4.7.0.28176
Fiji ImageJ	Wayne Rusband; National Institute of Health	https://imagej.net/software/fiji/

ACKNOWLEDGMENTS

This work was supported by funding by Institutional Research Concept RV067985904, the Czech Science Foundation [22-27301S]; MZE-RO0723; CARDIA, project EXCELES LX22NPO5104 funded by Next Generation EU; and by grant from Charles University GAUK 108624.

AUTHOR CONTRIBUTIONS

S.M., J.T. and A.S. designed experiments. S.M. cultivated primary patient PDAC cells from biopsy, performed PANC-1 cell viability assay, cytometry, immunocytochemistry, transfection, and fluorescence microscopy scanning of images. D.J. performed and analysed PLA assay, FISH, confocal scanning of images and analysed data from microscopy experiments. J.V. and L.J.L. performed TNT activation and TNT analysis. J.T., L.J.L., J.V. and M.H. analysed data from flow cytometry. P.D. performed cloning and verification of the HaloTag construct. M.B. and J.H. performed biopsies of PDAC patients and collected clinical data. S.M. and J.T. wrote the manuscript with input from all co-authors, all co-authors read and edited the final manuscript.

DECLARATION OF INTEREST

The authors declare no competing interests.

RESOURCE AVAILABILITY

Lead contact

Further information and requests for resources and reagents should be directed to and will be fulfilled by the lead contact, Jan Trnka (jan.trnka@lf3.cuni.cz)

Data and code availability

- All data reported in this paper is available at https://github.com/trnkaj/ribosomes.
- This paper reports original code available at https://github.com/trnkaj/ribosomes.
- Any additional information required to reanalyze the data reported in this paper is available from the lead contact upon request.

REFERENCES

1. Grossberg, A.J., Chu, L.C., Deig, C.R., Fishman, E.K., Hwang, W.L., Maitra, A., Marks, D.L., Mehta, A., Nabavizadeh, N., Simeone, D.M., et al. (2020). Multidisciplinary standards of care and recent progress in pancreatic ductal adenocarcinoma. CA Cancer J Clin *70*, 375–403. https://doi.org/10.3322/CAAC.21626.
2. Burris, H.A., Moore, M.J., Andersen, J., Green, M.R., Rothenberg, M.L., Modiano, M.R., Cripps, M.C., Portenoy, R.K., Storniolo, A.M., Tarassoff, P., et al. (2016). Improvements in survival and clinical benefit with gemcitabine as first-line therapy for patients with advanced pancreas cancer: a randomized trial. J Clin Oncol *15*, 2403–2413. https://doi.org/10.1200/JCO.1997.15.6.2403.
3. Conroy, T., Desseigne, F., Ychou, M., Bouché, O., Guimbaud, R., Bécouarn, Y., Adenis, A., Raoul, J.-L., Gourgou-Bourgade, S., de la Fouchardière, C., et al. (2011). FOLFIRINOX versus Gemcitabine for Metastatic Pancreatic Cancer. N Engl J Med *364*, 1817–1825. https://doi.org/10.1056/NEJMoa1011923.
4. Zuzčák, M., and Trnka, J. (2022). Cellular metabolism in pancreatic cancer as a tool for prognosis and treatment (Review). Int J Oncol *61*. https://doi.org/10.3892/IJO.2022.5383.
5. Dolfi, S.C., Li, L., Chan, -Ying, Qiu, J., Tedeschi, P.M., Bertino, J.R., Hirshfield, K.M., Oltvai, Z.N., and Vazquez, A. (2013). The metabolic demands of cancer cells are coupled to their size and protein synthesis rates. Cancer & Metabolism *1*, 1–13. https://doi.org/10.1186/2049-3002-1-20.
6. Donati, G., Montanaro, L., and Derenzini, M. (2012). Ribosome biogenesis and control of cell proliferation: p53 is not alone. Cancer Res *72*, 1602–1607. https://doi.org/10.1158/0008-5472.CAN-11-3992.
7. Prakash, V., Carson, B.B., Feenstra, J.M., Dass, R.A., Sekyrova, P., Hoshino, A., Petersen, J., Guo, Y., Parks, M.M., Kurylo, C.M., et al. (2019). Ribosome biogenesis during cell cycle arrest fuels EMT in development and disease. Nat Commun *10*. https://doi.org/10.1038/S41467-019-10100-8.
8. Flach, J., Bakker, S.T., Mohrin, M., Conroy, P.C., Pietras, E.M., Reynaud, D., Alvarez, S., Diolaiti, M.E., Ugarte, F., Forsberg, E.C., et al. (2014). Replication stress is a potent driver of functional

decline in ageing haematopoietic stem cells. Nature *512*, 198–202. https://doi.org/10.1038/NATURE13619.
9. Morral, C., Stanisavljevic, J., Hernando-Momblona, X., Mereu, E., Álvarez-Varela, A., Cortina, C., Stork, D., Slebe, F., Turon, G., Whissell, G., et al. (2020). Zonation of Ribosomal DNA Transcription Defines a Stem Cell Hierarchy in Colorectal Cancer. Cell Stem Cell *26*, 845-861.e12. https://doi.org/10.1016/J.STEM.2020.04.012.
10. Bywater, M.J., Poortinga, G., Sanij, E., Hein, N., Peck, A., Cullinane, C., Wall, M., Cluse, L., Drygin, D., Anderes, K., et al. (2012). Inhibition of RNA polymerase I as a therapeutic strategy to promote cancer-specific activation of p53. Cancer Cell *22*, 51–65. https://doi.org/10.1016/J.CCR.2012.05.019.
11. Cornelison, R., Dobbin, Z.C., Katre, A.A., Jeong, D.H., Zhang, Y., Chen, D., Petrova, Y., Llaneza, D.C., Steg, A.D., Parsons, L., et al. (2017). Targeting RNA-Polymerase I in Both Chemosensitive and Chemoresistant Populations in Epithelial Ovarian Cancer. Clin Cancer Res *23*, 6529–6540. https://doi.org/10.1158/1078-0432.CCR-17-0282.
12. Negi, S.S., and Brown, P. (2015). rRNA synthesis inhibitor, CX-5461, activates ATM/ATR pathway in acute lymphoblastic leukemia, arrests cells in G2 phase and induces apoptosis. Oncotarget *6*, 18094–18104. https://doi.org/10.18632/ONCOTARGET.4093.
13. Yu, P., Qu, N., Zhu, R., Hu, J., Han, P., Wu, J., Tan, L., Gan, H., He, C., Fang, C., et al. (2023). TERT accelerates BRAF mutant-induced thyroid cancer dedifferentiation and progression by regulating ribosome biogenesis. Sci Adv *9*. https://doi.org/10.1126/SCIADV.ADG7125.
14. Ariazi, J., Benowitz, A., De Biasi, V., Den Boer, M.L., Cherqui, S., Cui, H., Douillet, N., Eugenin, E.A., Favre, D., Goodman, S., et al. (2017). Tunneling Nanotubes and Gap Junctions-Their Role in Long-Range Intercellular Communication during Development, Health, and Disease Conditions. Front Mol Neurosci *10*. https://doi.org/10.3389/FNMOL.2017.00333.
15. Rustom, A., Saffrich, R., Markovic, I., Walther, P., and Gerdes, H.H. (2004). Nanotubular highways for intercellular organelle transport. Science *303*, 1007–1010. https://doi.org/10.1126/SCIENCE.1093133.
16. Austefjord, M.W., Gerdes, H.H., and Wang, X. (2014). Tunneling nanotubes: Diversity in morphology and structure. Commun Integr Biol *7*, e27934. https://doi.org/10.4161/CIB.27934.
17. Zurzolo, C. (2021). Tunneling nanotubes: Reshaping connectivity. Curr Opin Cell Biol *71*, 139–147. https://doi.org/10.1016/J.CEB.2021.03.003.
18. Hekmatshoar, Y., Nakhle, J., Galloni, M., and Vignais, M.L. (2018). The role of metabolism and tunneling nanotube-mediated intercellular mitochondria exchange in cancer drug resistance. Biochemical Journal *475*, 2305–2328. https://doi.org/10.1042/BCJ20170712.
19. Smith, I.F., Shuai, J., and Parker, I. (2011). Active Generation and Propagation of Ca2+ Signals within Tunneling Membrane Nanotubes. Biophys J *100*, L37–L39. https://doi.org/10.1016/J.BPJ.2011.03.007.
20. Abounit, S., Delage, E., and Zurzolo, C. (2015). Identification and characterization of tunneling nanotubes for intercellular trafficking. Curr Protoc Cell Biol *2015*, 12.10.1-12.10.21. https://doi.org/10.1002/0471143030.cb1210s67.
21. Murray, L.M.A., and Krasnodembskaya, A.D. (2019). Concise Review: Intercellular Communication Via Organelle Transfer in the Biology and Therapeutic Applications of Stem Cells. Stem Cells *37*, 14–25. https://doi.org/10.1002/STEM.2922.
22. Haimovich, G., Dasgupta, S., and Gerst, J.E. (2021). RNA transfer through tunneling nanotubes. Biochem Soc Trans *49*, 145–160. https://doi.org/10.1042/BST20200113.
23. Pepe, A., Pietropaoli, S., Vos, M., Barba-Spaeth, G., and Zurzolo, C. (2022). Tunneling nanotubes provide a route for SARS-CoV-2 spreading. Sci Adv *8*, 171. https://doi.org/10.1126/sciadv.abo0171.

24. Pinto, G., Saenz-De-Santa-Maria, I., Chastagner, P., Perthame, E., Delmas, C., Toulas, C., Moyal-Jonathan-Cohen, E., Brou, C., and Zurzolo, C. (2021). Patient-derived glioblastoma stem cells transfer mitochondria through tunneling nanotubes in tumor organoids. Biochem J *478*, 21–39. https://doi.org/10.1042/BCJ20200710.
25. Nakhle, J., Khattar, K., Özkan, T., Boughlita, A., Abba Moussa, D., Darlix, A., Lorcy, F., Rigau, V., Bauchet, L., Gerbal-Chaloin, S., et al. (2023). Mitochondria Transfer from Mesenchymal Stem Cells Confers Chemoresistance to Glioblastoma Stem Cells through Metabolic Rewiring. Cancer Res Commun *3*, 1041–1056. https://doi.org/10.1158/2767-9764.CRC-23-0144.
26. Saha, T., Dash, C., Jayabalan, R., Khiste, S., Kulkarni, A., Kurmi, K., Mondal, J., Majumder, P.K., Bardia, A., Jang, H.L., et al. (2021). Intercellular nanotubes mediate mitochondrial trafficking between cancer and immune cells. Nature Nanotechnol *17*, 98–106. https://doi.org/10.1038/s41565-021-01000-4.
27. Kretschmer, A., Zhang, F., Somasekharan, S.P., Tse, C., Leachman, L., Gleave, A., Li, B., Asmaro, I., Huang, T., Kotula, L., et al. (2019). Stress-induced tunneling nanotubes support treatment adaptation in prostate cancer. Sci Rep *9*, 1–13. https://doi.org/10.1038/s41598-019-44346-5.
28. Lu, J., Zheng, X., Li, F., Yu, Y., Chen, Z., Liu, Z., Wang, Z., Xu, H., and Yang, W. (2017). Tunneling nanotubes promote intercellular mitochondria transfer followed by increased invasiveness in bladder cancer cells. Oncotarget *8*, 15539–15552. https://doi.org/10.18632/ONCOTARGET.14695.
29. Desir, S., O'hare, P., Vogel, R.I., Sperduto, W., Sarkari, A., Dickson, E.L., Wong, P., Nelson, A.C., Fong, Y., Steer, C.J., et al. (2018). Chemotherapy-Induced Tunneling Nanotubes Mediate Intercellular Drug Efflux in Pancreatic Cancer. Sci Rep *8*, 9484. https://doi.org/10.1038/s41598-018-27649-x.
30. Lou, E., Fujisawa, S., Morozov, A., Barlas, A., Romin, Y., Dogan, Y., Gholami, S., Moreira, A.L., Manova-Todorova, K., and Moore, M.A.S. (2012). Tunneling Nanotubes Provide a Unique Conduit for Intercellular Transfer of Cellular Contents in Human Malignant Pleural Mesothelioma. PLoS One *7*, e33093. https://doi.org/10.1371/JOURNAL.PONE.0033093.
31. Desir, S., Dickson, E.L., Vogel, R.I., Thayanithy, V., Wong, P., Teoh, D., Geller, M.A., Steer, C.J., Subramanian, S., Lou, E., et al. (2016). Tunneling nanotube formation is stimulated by hypoxia in ovarian cancer cells. Oncotarget *7*, 43150–43161. https://doi.org/10.18632/ONCOTARGET.9504.
32. Pinto, G., Brou, C., and Zurzolo, C. (2020). Tunneling Nanotubes: The Fuel of Tumor Progression? Trends Cancer *6*, 874-–888. 10.1016/j.trecan.2020.04.012.
33. Hanna, S.J., McCoy-Simandle, K., Leung, E., Genna, A., Condeelis, J., and Cox, D. (2019). Tunneling nanotubes, a novel mode of tumor cell–macrophage communication in tumor cell invasion. J Cell Sci *132*, jcs223321. https://doi.org/ 10.1242/jcs.223321.
34. Jansova, D., Tetkova, A., Koncicka, M., Kubelka, M., and Susor, A. (2018). Localization of RNA and translation in the mammalian oocyte and embryo. PLoS One *13*, e0192544. https://doi.org/10.1371/JOURNAL.PONE.0192544.
35. Cheng, S., Altmeppen, G., So, C., Welp, L.M., Penir, S., Ruhwedel, T., Menelaou, K., Harasimov, K., Stützer, A., Blayney, M., et al. (2022). Mammalian oocytes store mRNAs in a mitochondria-associated membraneless compartment. Science *378*, eabq4835. https://doi.org/10.1126/science.abq4835.
36. Klinge, S., Voigts-Hoffmann, F., Leibundgut, M., and Ban, N. (2012). Atomic structures of the eukaryotic ribosome. Trends Biochem Sci *37*, 189–198. https://doi.org/10.1016/j.tibs.2012.02.007
37. Smith, P.R., Loerch, S., Kunder, N., Stanowick, A.D., Lou, T.F., Campbell, Z.T. (2021). Functionally distinct roles for eEF2K in the control of ribosome availability and p-body abundance. Nat Commun 23;12(1):6789. doi: 10.1038/s41467-021-27160-4.
38. Gallo, S., Beugnet, A., and Biffo, S. (2011). Tagging of functional ribosomes in living cells by HaloTag® technology. In Vitro Cell Dev Biol Anim *47*, 132–138. https://doi.org/10.1007/S11626-010-9370-7.

39. Burger, K., Mühl, B., Harasim, T., Rohrmoser, M., Malamoussi, A., Orban, M., Kellner, M., Gruber-Eber, A., Kremmer, E., Hölzel, M., et al. (2010). Chemotherapeutic drugs inhibit ribosome biogenesis at various levels. J Biol Chem *285*, 12416–12425. https://doi.org/10.1074/JBC.M109.074211.
40. Spees, J.L., Olson, S.D., Whitney, M.J., and Prockop, D.J. (2006). Mitochondrial transfer between cells can rescue aerobic respiration. Proc Natl Acad Sci U S A *103*, 1283–1288. https://doi.org/10.1073/PNAS.0510511103.
41. Cho, Y.M., Kim, J.H., Kim, M., Park, S.J., Koh, S.H., Ahn, H.S., Kang, G.H., Lee, J. Bin, Park, K.S., and Lee, H.K. (2012). Mesenchymal stem cells transfer mitochondria to the cells with virtually no mitochondrial function but not with pathogenic mtDNA mutations. PLoS One *7*, e32778. https://doi.org/10.1371/JOURNAL.PONE.0032778.
42. Tan, A.S., Baty, J.W., Dong, L.F., Bezawork-Geleta, A., Endaya, B., Goodwin, J., Bajzikova, M., Kovarova, J., Peterka, M., Yan, B., et al. (2015). Mitochondrial genome acquisition restores respiratory function and tumorigenic potential of cancer cells without mitochondrial DNA. Cell Metab *21*, 81–94. https://doi.org/10.1016/J.CMET.2014.12.003.
43. Ippolito, L., Morandi, A., Taddei, M.L., Parri, M., Comito, G., Iscaro, A., Raspollini, M.R., Magherini, F., Rapizzi, E., Masquelier, J., et al. (2019). Cancer-associated fibroblasts promote prostate cancer malignancy via metabolic rewiring and mitochondrial transfer. Oncogene *38*, 5339–5355. https://doi.org/10.1038/S41388-019-0805-7.
44. Khalaileh, A., Dreazen, A., Khatib, A., Apel, R., Swisa, A., Kidess-Bassir, N., Maitra, A., Meyuhas, O., Dor, Y., and Zamir, G. (2013). Phosphorylation of ribosomal protein S6 attenuates DNA damage and tumor suppression during development of pancreatic cancer. Cancer Res *73*, 1811–1820. https://doi.org/10.1158/0008-5472.CAN-12-2014.
45. Tang, Y., Luo, J., Zhou, Y., Zang, H., Yang, Y., Liu, S., Zheng, H., Ma, J., Fan, S., and Wen, Q. (2022). Overexpressed p-S6 associates with lymph node metastasis and predicts poor prognosis in non-small cell lung cancer. BMC Cancer *22*, 564. https://doi.org/10.1186/S12885-022-09664-4.
46. Weidenauer, K., Schmidt, C., Rohde, C., Pauli, C., Blank, M.F., Heid, D., Waclawiczek, A., Corbacioglu, A., Göllner, S., Lotze, M., et al. (2023). The ribosomal protein S6 kinase alpha-1 (RPS6KA1) induces resistance to venetoclax/azacitidine in acute myeloid leukemia. Leukemia *37*, 1611–1625. https://doi.org/10.1038/s41375-023-01951-8.
47. Awasthi, N., Yen, P.L., Schwarz, M.A., and Schwarz, R.E. (2012). The efficacy of a novel, dual PI3K/mTOR inhibitor NVP-BEZ235 to enhance chemotherapy and antiangiogenic response in pancreatic cancer. J Cell Biochem *113*, 784–791. https://doi.org/10.1002/JCB.23405.
48. De, A., Jacobson, B.A., Peterson, M.S., Jay-Dixon, J., Kratzke, M.G., Sadiq, A.A., Patel, M.R., and Kratzke, R.A. (2018). 4EGI-1 represses cap-dependent translation and regulates genome-wide translation in malignant pleural mesothelioma. Invest New Drugs *36*, 217–229. https://doi.org/10.1007/s10637-017-0535-z.
49. Yang, C., Endoh, M., Tan, D.Q., Nakamura-Ishizu, A., Takihara, Y., Matsumura, T., Suda, T. (2021). Mitochondria transfer from early stages of erythroblasts to their macrophage niche via tunnelling nanotubes. Br J Haematol 193(6):1260-1274. doi: 10.1111/bjh.17531.
50. Wang, F., Chen, X., Cheng, H., Song, L., Liu, J., Caplan, S., Zhu, L., Wu, J.Y. (2021). MICAL2PV suppresses the formation of tunneling nanotubes and modulates mitochondrial trafficking. EMBO Rep. 5;22(7):e52006. doi: 10.15252/embr.202052006.
51. Willms, E., Johansson, H.J., Mäger, I., Lee, Y., Blomberg, K.E., Sadik, M., Alaarg, A., Smith, CI., Lehtiö, J., El Andaloussi, S., Wood, M.J., Vader, P. (2016). Cells release subpopulations of exosomes with distinct molecular and biological properties. Sci Rep 2;6:22519. doi: 10.1038/srep22519.
52. Dabbah, M., Lishner, M., Jarchowsky-Dolberg, O., Tartakover-Matalon, S., Brin, Y.S., Pasmanik-Chor, M., Neumann, A., Drucker, L. (2021). Ribosomal proteins as distinct "passengers" of microvesicles: new semantics in myeloma and mesenchymal stem cells' communication. Transl Res 236:117-132. doi: 10.1016/j.trsl.2021.04.002.

53. Ellis, B., Haaland, P., Hahne, F., Le Meur, N., Gopalakrishnan, N., Spidlen, J., Jiang, M., Finak, G. (2024). flowCore: flowCore: Basic structures for flow cytometry data. R package version 2.18.0.
54. Van, P., Jiang, W., Gottardo, R., Finak, G. (2018). ggCyto: next generation open-source visualization software for cytometry. Bioinformatics 15;34(22):3951-3953. https://doi.org/10.1093/bioinformatics/bty441

FIGURES

Figure 1. Tunnelling nanotubes form in 2D cultures of primary PDAC and in PANC-1 cell line treated with gemcitabine. (A) Cells in 2D cultures of fine-needle biopsy samples from a PDAC patient BJPN0015 develop TNTs. (B) PANC-1 cell line increases the number of TNTs in response to gemcitabine. Green, CellMask Green (actin); red, TMRM (mitochondria); blue, Hoechst 33342 (DNA). (C) Linear model of the dose-dependence of TNT formation on gemcitabine concentration. (D) Confocal 3D reconstruction of one TNT between PANC-1 cells with depth coding showing that the TNT is above the substrate. Further images in Supplementary figure S1.

Figure 2. Ribosomal components, mRNA and fully assembled ribosomes detected in tunneling nanotubes. Ribosomal components 5.8S rRNA (A), ribosomal protein S6 (B), ribosomal protein L24 (C), poly-A mRNA (D), complete ribosomes (E) and ribosomal protein S9 (F) found in TNTs formed between PANC-1 cells in culture after a 48-hour exposure to 0.5 µM gemcitabine. 5.8S rRNA (G, J) and complete ribosomes (H, K) detected in TNTs formed between patient-derived cells in culture, accompanied by cytokeratin 19 (I) and vimentin (L). Images from a confocal microscope (*) and from a fluorescent microscope (#). Further images in Supplementary figure S2, S4A, S4B, S5A, S5B, S7A, S7B.

Figure 3. Ribosomal component RPS9 is transported between cells via TNTs and incorporated into ribosomes. HaloTag-labelled RPS9 is transported to untransfected PANC-1 cells labelled with a blue CellTrace™ Violet stain (A) or to PANC-1 cells transfected with nuclear targeted GFP (B). Complete ribosomes detected in TNTs between PANC-1 cells by the RPS9-RPL24 proximity ligation assay (C) or by the HaloTag-RPS9-RPL24 proximity ligation assay, showing the incorporation of the labelled RPS9 into complete ribosomes (maximum projection image, D), and shown to be transferred to untransfected CellTrace Violet cells and found in complete ribosomes (E). Transfer of HaloTag-RPS9 to untransfected CellTrace Violet cells detected by flow cytometry as double-positive cells (F) is increased by sub-IC50 exposure to gemcitabine (mean counts of three eperiments shown as lines in the summary graph). Images from a confocal microscope (*) and from a fluorescent microscope (#). Further images in Supplementary figure S3, S8, S9 and all flow cytometry dot plots and singlets gate sensitivity analyses are shown in Supplementary figure S11.

Video 1. Live cell imaging of HaloTag- RPS9 transport in TNTs between PANC-1 cells. A movement of the HaloTag labelled RPS9 within TNTs formed between PANC-1 cells in culture after a 48 hours exposure to 0.5 µM gemcitabine (3.873 seconds per frame).

A Tumor samples form TNTs in 2D culture

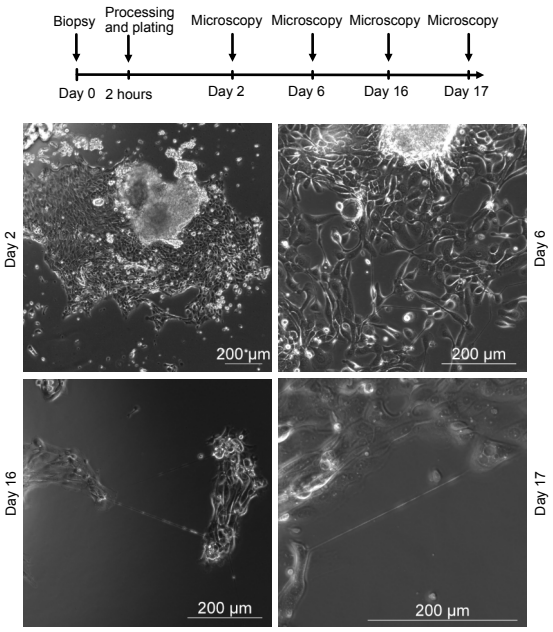

B Gemcitabine induces TNT formation

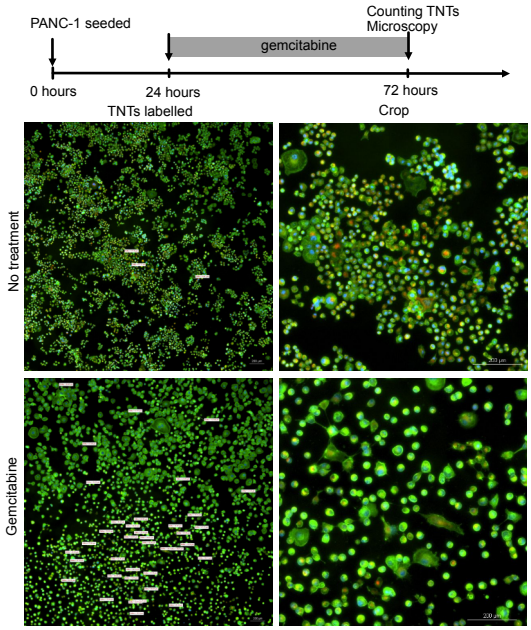

C Gemcitabine induces TNTs in PANC-1

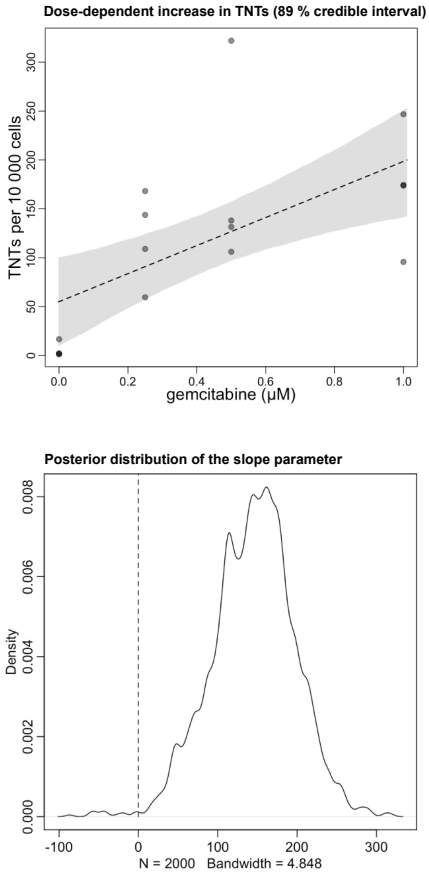

D Depth-coded 3D confocal image of a TNT

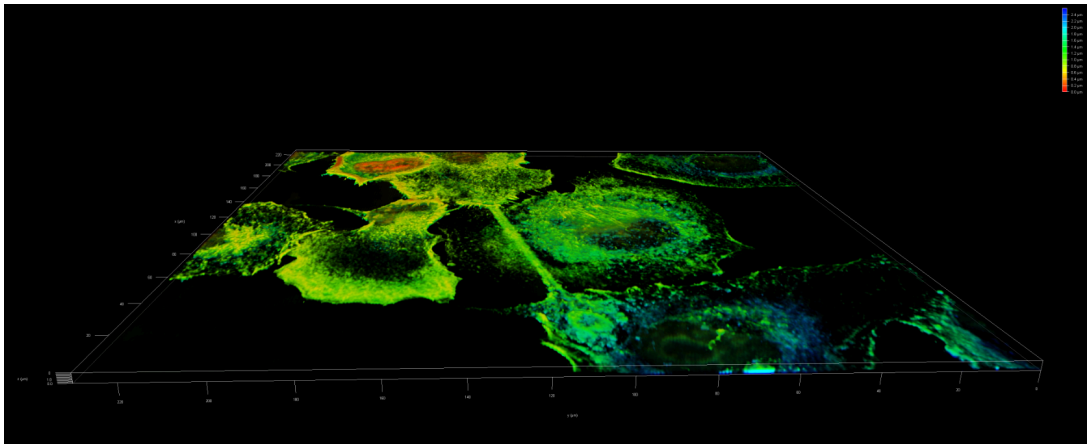

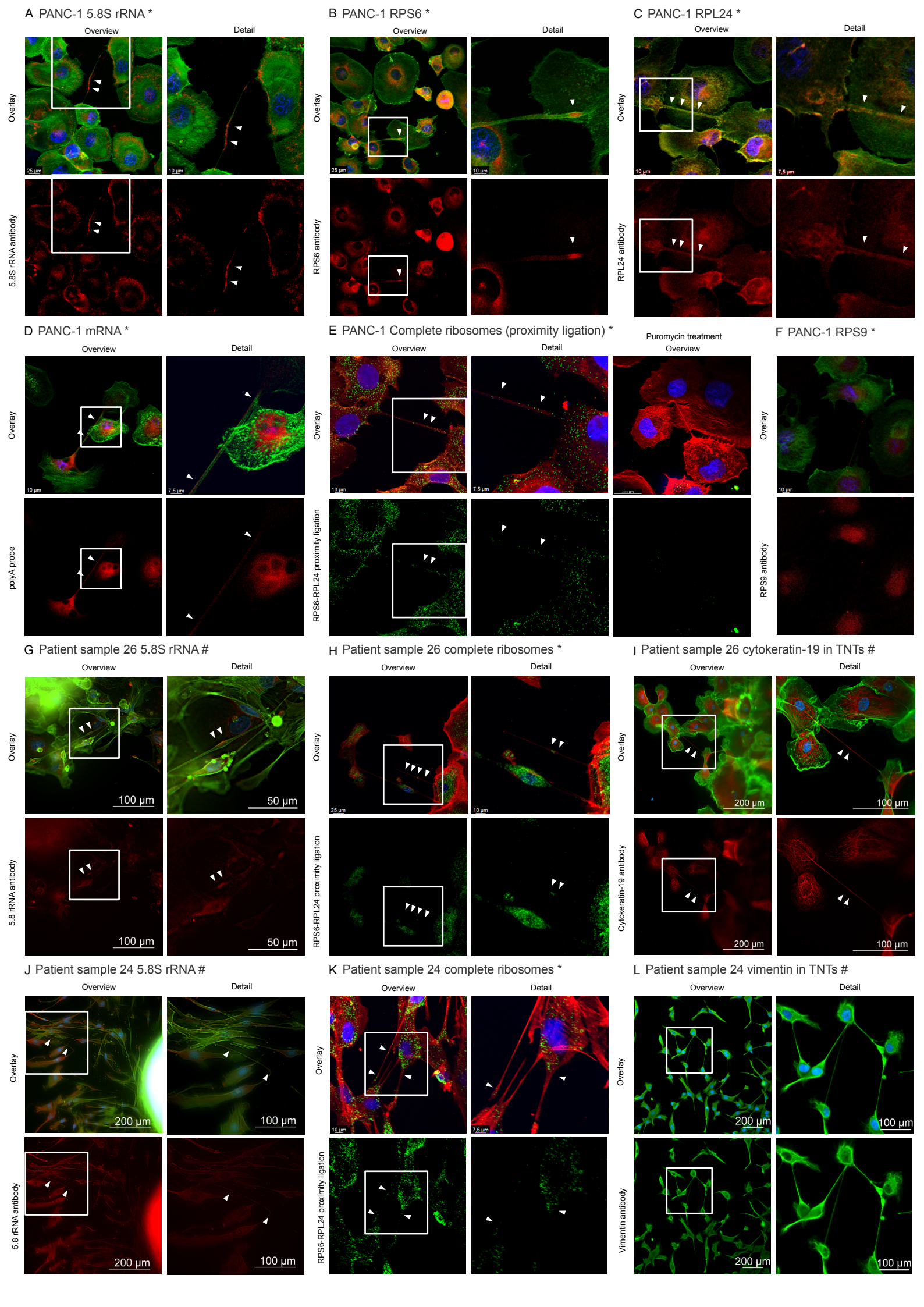
A PANC-1 5.8S rRNA *
Overview
Detail
Overlay
5.8S rRNA antibody
B PANC-1 RPS6 *
Overview
Detail
Overlay
RPS6 antibody
C PANC-1 RPL24 *
Overview
Detail
Overlay
RPL24 antibody
D PANC-1 mRNA *
Overview
Detail
Overlay
polyA probe
E PANC-1 Complete ribosomes (proximity ligation) *
Overview
Detail
Puromycin treatment
Overview
Overlay
RPS6-RPL24 proximity ligation
F PANC-1 RPS9 *
Overlay
RPS9 antibody
G Patient sample 26 5.8S rRNA #
Overview
Detail
Overlay
5.8 rRNA antibody
100 µm
50 µm
H Patient sample 26 complete ribosomes *
Overview
Detail
Overlay
RPS6-RPL24 proximity ligation
I Patient sample 26 cytokeratin-19 in TNTs #
Overview
Detail
Overlay
Cytokeratin-19 antibody
200 µm
100 µm
J Patient sample 24 5.8S rRNA #
Overview
Detail
Overlay
5.8 rRNA antibody
200 µm
100 µm
K Patient sample 24 complete ribosomes *
Overview
Detail
Overlay
RPS6-RPL24 proximity ligation
L Patient sample 24 vimentin in TNTs #
Overview
Detail
Overlay
Vimentin antibody
200 µm
100 µm

A Transport of HaloTag RPS9 (red) to untransfected cells (blue) in PANC- 1 #

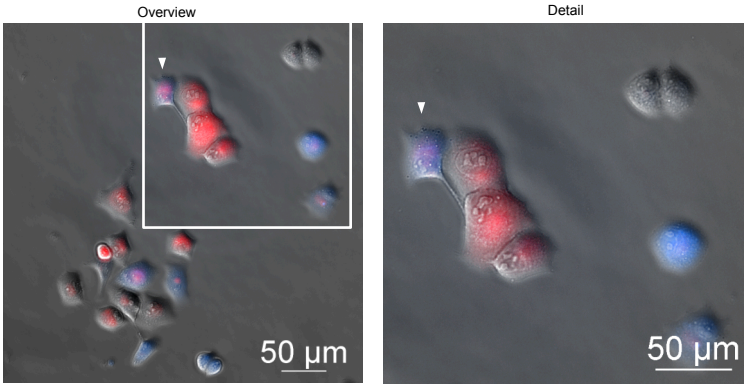

B Transport of HaloTag RPS9 (red) to nuclear GFP cells (green) in PANC- 1 #

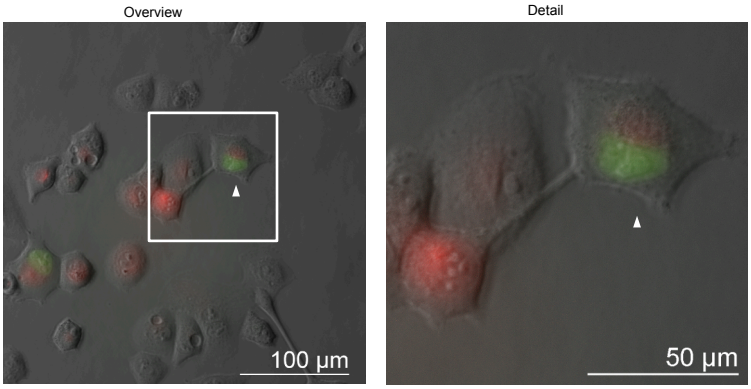

C Proximity ligation assay RPS9-RPL24 in PANC- 1 *

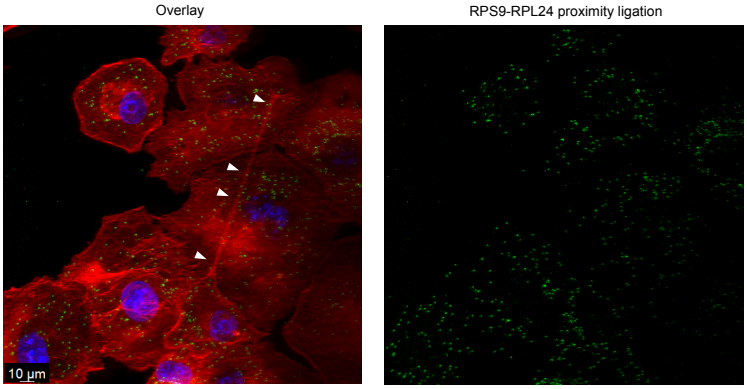

D Incorporation of HaloTag-RPS9 into ribosomes in PANC- 1 *

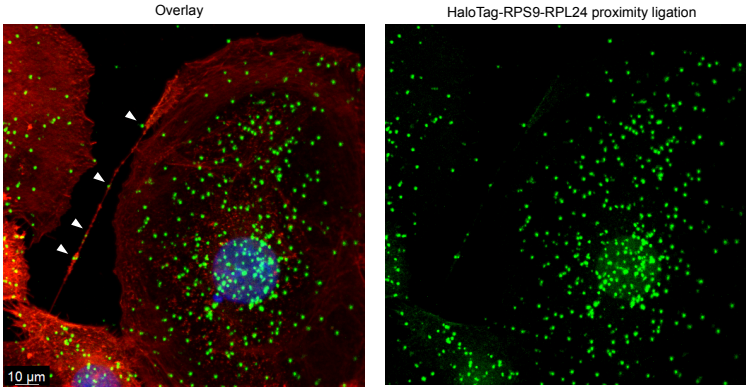

E Proximity ligation assay HaloTag-RPS9-RPL24 in CellTrace Violet recipient cells*

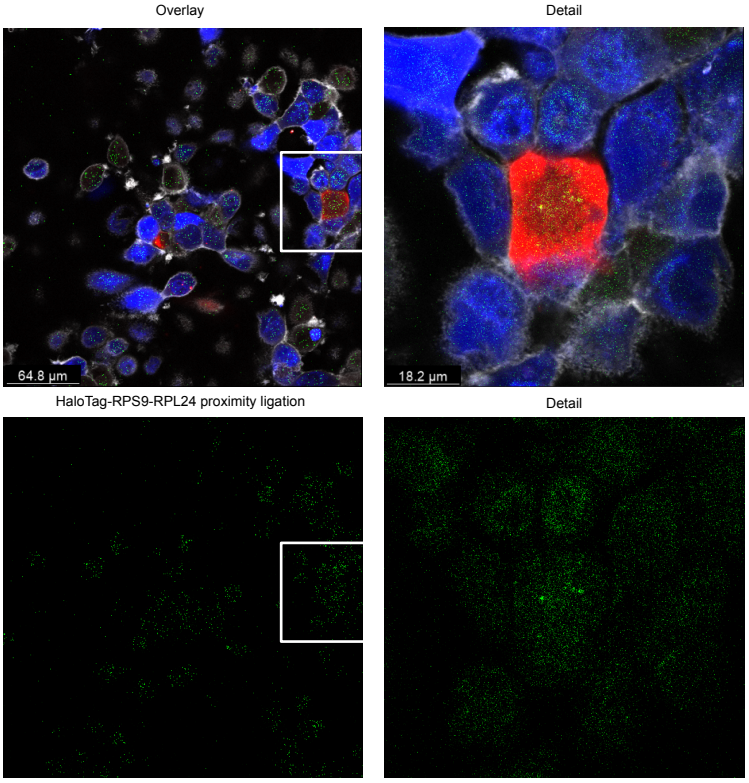
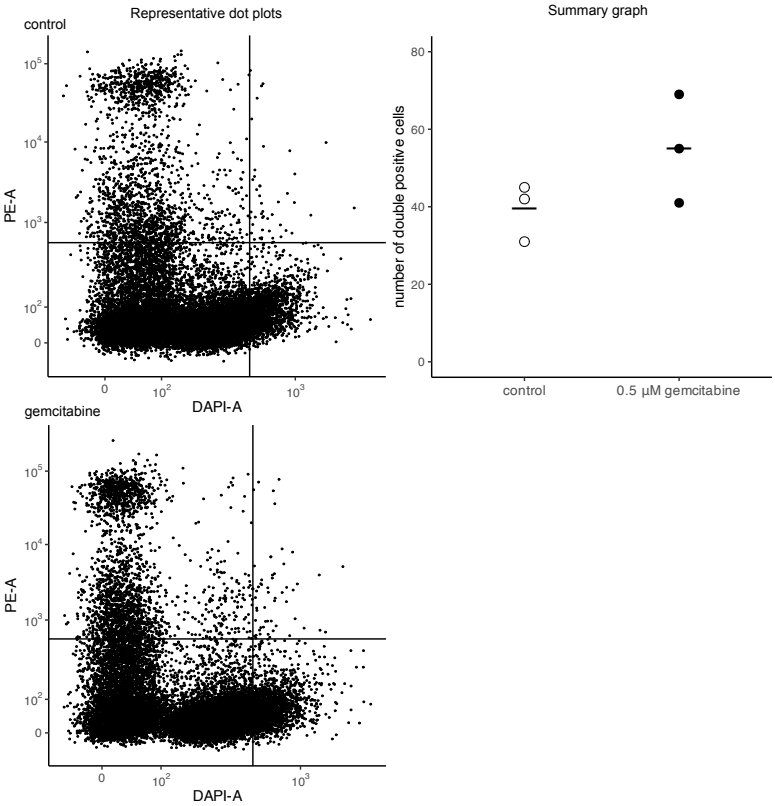
F Flow cytometry HaloTag-RPS9-RPL24 in CellTrace Violet recipient cells